IOP Conf. Series: Materials Science and Engineering **454** (2018) 012033 doi:10.1088/1757-899X/454/1/012033

Enhanced Photoelectrochemical Water Splitting of Hydrothermally-Grown ZnO and Yttrium-doped ZnO NR Arrays

Amin K. Qasim[1,*], Lazgin A. Jamil[2] and Qiao chen[3]

[1*]Faculty of Science, Department of Chemistry, University of Zakho, Duhok, Kurdistan Region, Iraq.
[2]Faculty of Science, Department of Chemistry, University of Zakho, Duhok, Kurdistan Region, Iraq.
[3]School of Life Sciences, Department of Chemistry, University of Sussex, Brighton, BN1 9QJ, UK.
[*]E-Mail:amin.qasim@uoz.edu.krd

Abstract. Undoped and Y doped ZnO nanorods (YZO NRs) were prepared by hydrothermal method. The as-prepared ZnO and YZO NRs with different Y/Zn molar ratios were used as anodes for electrochemical water splitting. Then, photoelectrochemical (PEC) water splitting performances of YZO NRs were tested. When compared with pristine ZnO NRs, the photocurrent density generated with yttrium doped zinc oxide NR as electrode was higher(1.2 mA cm^{-2}) than that obtained with pristine ZnO NRs (0.25 mA cm^{-2}), at 0.2 V vs. Ag/ AgCl using samples of 1.2 mol % of yttrium. This performance corresponds to calculated photo-conversion efficiency of 0.40%, at a low potential (-0.38V vs Ag/AgCl) of the non-doped ZnO NR film.

Keuwords: Yttrium doped zinc oxide nanorod, Sol gel deposition, Structural properties

1. Introduction

Zinc oxide (ZnO) is an important material due to its exceptional wide direct band gap (3.37 eV at 300 K), high exciton binding energy (60 meV), and excellent chemical and thermal stabilities [1]. ZnO nanostructures around the size of individual atoms and molecules exhibit both physical and chemical properties, which are quite different from those of bulk size materials [2]. Owing to these properties, it has been investigated for low voltage and short wavelength electro-optical devices such as light emitting diodes [3], UV lasers [4], chemical sensors [5] and solar cells [6].

The one-dimensional (1D) ZnO nanostructures, including nanotubes [7], nanowires [8] and nanorods [9] have been studied extensively for their unique properties, large surface area and short diffusion lengths for photogenerated minority carriers and potential applications in nano devices [10]. However, the photoconversion efficiency of ZnO nanomaterials is significantly limited due to its large band gap (3.37 eV). And it only absorb light in the UV region and rapid charge recombination due to the high density of trap states [11]. Thus, many efforts have been focused on to increase the absorption of ZnO in the visible region [12, 13].

Doping is an effective way to improve the properties of ZnO nanostructures, various types of extrinsic dopants, for instance, metal cations [14] and non-metal anions have been introduced into ZnO for enhancing the photoconversion efficiency. Recently; Yttrium doped ZnO (YZO) NRs has been of interest because Y improves the optical and the electrical properties of ZnO NRs [17, 18]. The major

benefits of Yttrium doping are (i) Yttrium doping decreases the energy band gap of ZnO [18], (ii) Y^{3+} surface enhances hinders crystallite growth and (iii) the surface segregation of Y^{3+} promotes oxygen vacancies creation [19]. On this basis, we have chosen Yttrium as dopant.

2. Experimental

2.1. Preparation of Undoped ZnO and Yttrium-Doped ZnO (YZO) NRs

In a typical synthesis, the process includes two main stages: seeding and growth processes
1. The seeding solution was prepared by the sol-gel spin coating technique, by dissolving 0.219 gm of Zinc Acetate Dehydrate (Alfa Aesar) (in 10.0 ml of DI water and is magnetically stirred for two hrs to form a 0.10 M seeding solution. The samples were spinned coated (speed~800 rpm, for time~40 s) the sample was annealed at 300 ^{o}C for 5 min to improve the crystal quality and to evaporate the solvent and to remove the organic residues, with the seeding solution followed by post annealing at 350°C for 20 min in order to convert the zinc acetate into ZnO seeds. 2. The growth solution prepared by hydrothermal process was prepared by dissolving 0.136 gm of zinc chloride anhydrous (98%) (Sigma Aldrich), in 10 ml of DI water to yield a 0.10 M solution. 3. For YZO nanostructures, different concentrations of yttrium nitrate hexahydrate (Alfa Aesar) with Y/Zn mole percentage of 0.4, 0.8, 1.2 and 2.2% were prepared. While magnetically stirring, a 0.5 ml of ammonia solution (25%) (Alfa Aesar) was added drop by drop into the growth solution to increase the solution pH to 10.0. The solution became milky due to the formation of Zn $(OH)_2$ sol-gel. Then, 8 ml of the as-prepared nutrient solution was poured into a 10 ml Teflon vessel with a seeded FTO glass immersed into the reaction solution. The sealed hydrothermal vessel was heated in an oven at 90 °C for 130 min. 4. The vessel was cooled down to room temperature. The as-grown sample was rinsed with DI water three times and dried at room temperature, and then became ready for characterization.

3. Results and Discussions

3.1. Morphology Analysis

Figure 1 (A-E) displays the top-view SEM images of the ZnO and Y-doped ZnO NRs samples synthesized by hydrothermal method with a different mole percentage of yttrium 0, 0.4, 0.8, 1.2 and 2.2%, respectively. It is found that the Y doping mol % has a significant influence on the surface morphology of the ZnO NRs.
Different dopants will form different charged complex ions in the nutrient solutions, which will cause a change in the growth direction of the NRs, either along the (002) top face or (100) sidewalls. This is because the ZnO (002) plane is negatively charged and (100) is positively charged [22]. Yttrium is technically classified as a transition metals; however it tolerates some similarities to group 13 elements which will form negatively charged complexes via the coordination of hydroxide ions, prohibiting the growth along the positively charged (100) plane. The morphology of YZO NRs is slightly different. As increased in the Y/Zn molar ratios, the length of the NRs increases and the average diameter of the NRs are decreased, forming needle-like ZnO nanostructures.

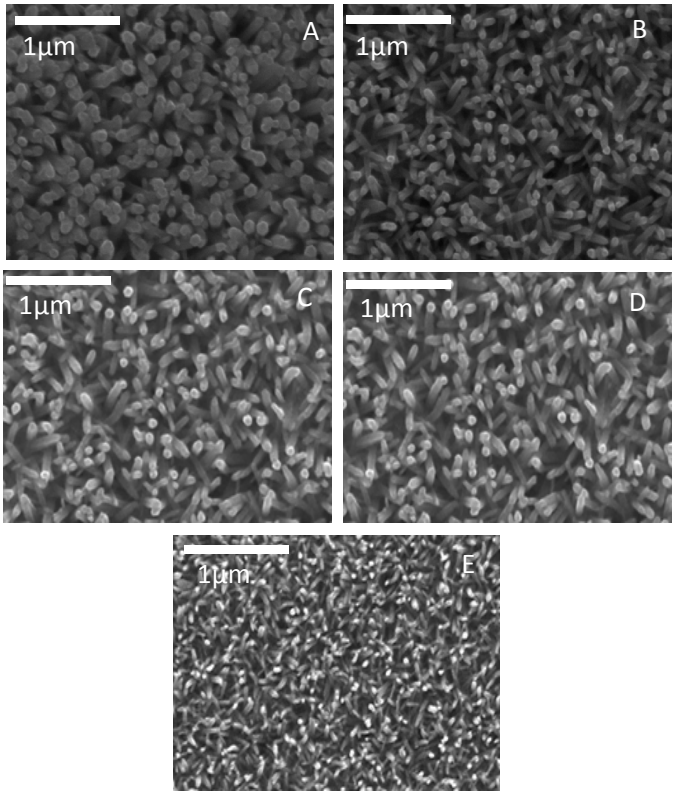

Figure 1. SEM images of ZnO NRs arrays and Y-doped ZnO NRs films grown on FTO substrate. ZnO NRs and YZO NRs grow at 90°C for 130 minutes with different dopant mole fraction in reactive solutions. (A) 0, (B) 0.4, (C) 0.8, (D) 1.2, and (E) 2.2 mol%.

Figure 2 shows the influence of Y doping on NRs size distribution. The average diameter of ZnO and YZO NRs are 198.4, 167.5, 153.8, 135.2 and 96.2 nm, the crystal domain size of ZnO nanorods (25.8, 25.1, 23.7, 25.3 and 25.6 nm) is calculated using the full width at half-maximum (FWHM) (0.310°, 0.382°, 0.401°, 0.362° and 0.322°) of the (002) peak and the Scherrer's relation $D = \frac{K\lambda}{\beta \cos\theta}$, where D is the crystal domain size, K is the shape factor (0.89 in this work), λ is the wavelength of the X-ray source (Cu target, λ = 1.541 Å), θ is the Bragg angle of the diffraction peak (in degrees) and β is the line width of the diffraction peak corrected for instrument broadening (in radians).

Average crystallite size is remarkably decreased from 25.8 to 23.7 nm by Y doping from 0.0 to 0.8 %. At higher Y doping, it increases from 25.3 nm (Y = 1.2 mol) to 25.6 nm (Y = 2.2 mol). Yttrium-doped ZnO shows the smaller crystalline size than un-doped ZnO. The change in FWHM reflects the reduction of crystalline size. The noticed reduction in the particle size is mainly due to the distortion in the host ZnO lattice by the foreign atom Y^{3+}. It can be seen that the average diameters decrease as the Yttrium % content increased from zero to 2.2 % as shown in Figure 3 (B).

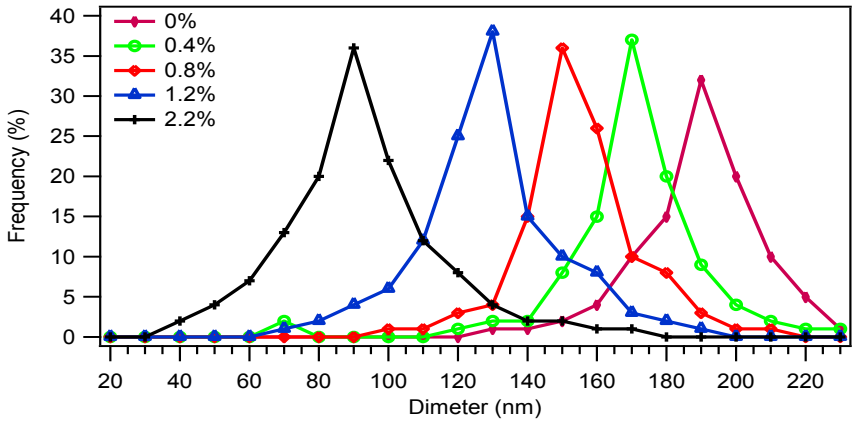

Figure 2. Diameter distributions of ZnO NRs and YZO NRs arrays prepared on an FTO substrate with different Y molar percentages of (A) 0, (B) 0.4, (C) 0.8, (D) 1.2, and (E) 2.2 mol% in the growth solutions.

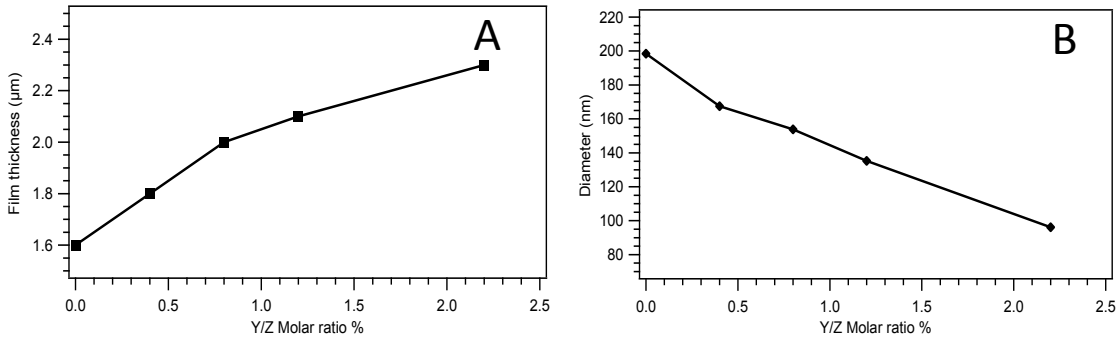

Figure 3. (A) Plots of film thickness and (B) Average diameter as a function of Y/Zn molar percentage.

Figure 4 depicts the cross section SEM image of ZnO and YZO NRs with the different percentages of Y 0, 0.4, 0.8, 1.2, 2.2% (A-E), respectively. Figure 4 B-E shows that as the Y mol% in the growth solution increases, the whole length of the Y-doped ZnO NRs also increases. However, the average length of ZnO and YZO NRs as measured in Figure 4(A-E) is 1.60, 1.77, 1.90, 2.07 and 2.02 μm respectively. This revealed that the Y doping had significant influence on the length of the NRs; also which respect to the non-doped ZnO NRs film, there is an obvious change in the length of the NRs after the incorporation of yttrium.

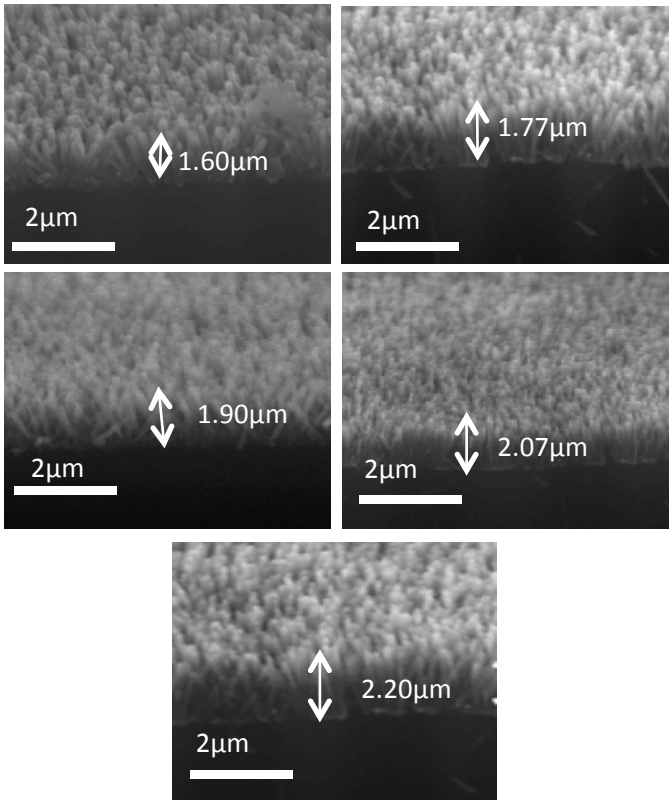

Figure 4. Cross section SEM image of Y-doped ZnO Nanorods grown on FTO substrate at different molar percentage of Y (A) 0, (B) 0.4, (C) 0.8, (D) 1.2, and (E) 2.2 mol% in the growth solutions.

3.2. Structural Studies of ZnO NRs and Y-Doped ZnO NRs

The X-ray diffraction patterns of undoped and Y-doped ZnO NRs are shown in Figure 5, they are used to study the crystal structure and crystal orientation of the samples. The XRD pattern clearly shows the crystalline nature with peaks corresponding to the peaks at the position of 31.51°, 34.60°, 36.42°, 47.70° and 63.98° matching to (100), (002), (101), (102) and (103) crystal planes. The diffraction peaks in the XRD spectra reveal that all the investigated samples have typical hexagonal wurtzite structures. The diffraction data analysis is in good agreement with the standard JCPDS file for ZnO (JCPDS 36-1451) [23]. No secondary phase is detected through the Y- doped ZnO NRs, which means that some Y^{3+} ions would uniformly substitute into the Zn^{2+} sites or interstitial sites in the ZnO lattice. Figure 5 being preferred (002) orientation, crystal plane, this suggests that the c-axis of the NRs is perpendicular to the substrate.

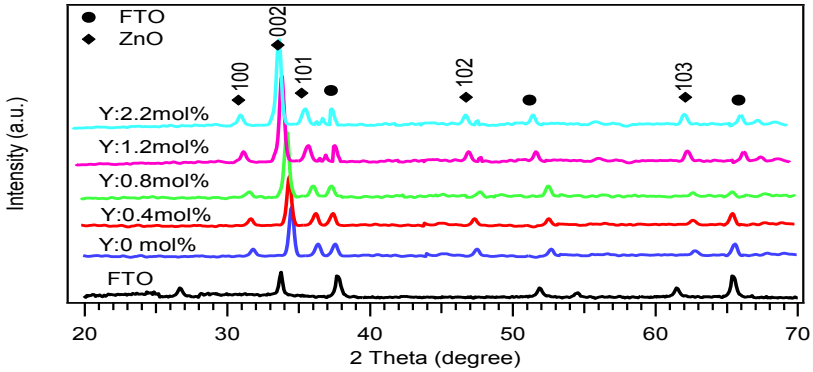

Figure 5. X-ray diffraction of ZnO and Y-doped ZnO nanorod films with varying doping concentration grown on FTO substrate. (a) 0, (b) 0.4, (c) 0.8, (d) 1.2, and (e) 2.2 mol%.

Figure 6 A shows that the diffraction peak gradually shifts towards the smaller angle from 34.60° to 34.15° when the Y-doped Zn molar percentage in the growth solution is increased from 0.4 to 2.2 %. Such a shift indicates that there is a systematic increase in ZnO lattice parameters as well as a gradual decrease of 2θ values with the Y/Zn molar ratio as shown in Figure 6 B. Consistently, the c-axis lattice constants of the thin films increased from (5.2130 A° to 5.2153A°) with increasing yttrium concentration, which may be due to the fact that the ionic radius Y^{3+} (1.015 Å) is larger than that of Zn^{2+} (0.74 Å) [24]. The variation of the c-axis lattice constant additional suggests that Y^{3+} ions replace the Zn^{2+} lattice sites or interstitial sites in the NRs films.

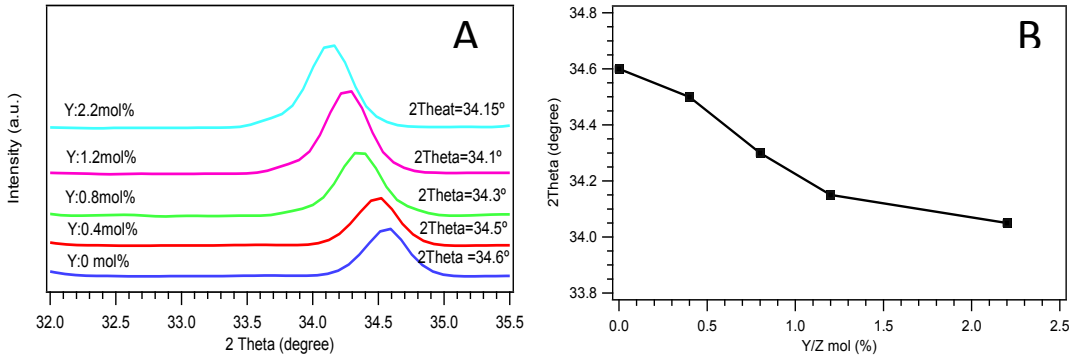

Figure 6. (A) The shift X-ray diffraction peaks of YZO Nanorods along (002) plane towards the lower diffraction angle. And (B) shows the variation of peak position 2θ as a function of Y mol%.

3.3. UV-Visible and Optical Properties

The UV-Visible optical absorption spectra of ZnO NRs and YZO NRs were carried out at room temperature from 350 to 500 nm as shown in Figure 7. In order to investigate the influence of Y doping and how the defects and dopants affect the electronic structures of ZnO NRs. In these cases, the samples were prepared on glass substrates, the absorption spectra were observed at 371, 374, 377, 378 and 382 nm for ZnO NRs and YZO NRs with Y/Zn molar percentages of 0, 0.4, 0.8, 1.2 and 2.2, respectively. The spectra show that the absorption around 350-400 nm reveals a blue shift with Y-doping. This blue shift could be ascribed to the formation of new donor centers [23], and the formation of shallow levels or sub band inside the band gap due to the incorporation of doping ions Y^{3+} [26]. These levels could act to capture electrons, which facilitates electronic transitions from the valance band to these levels and then to the conduction band, and also prevent electron-hole pair recombination.

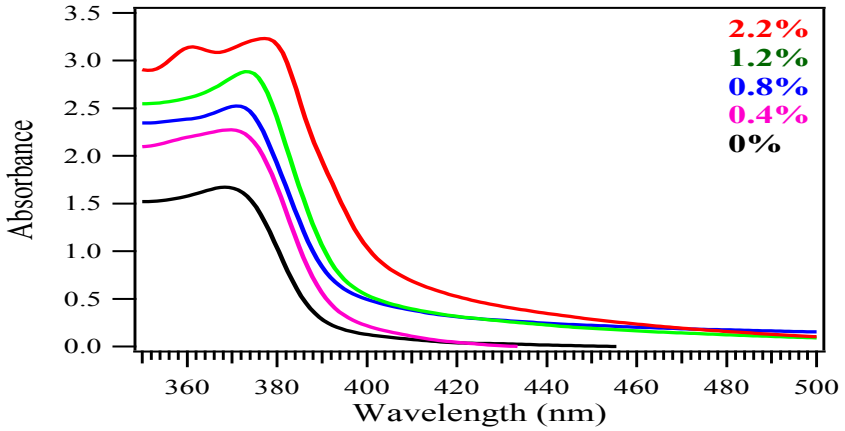

Figure 7. UV-Vis absorption spectra of ZnO NRs and YZO NRs Synthesized by Hydrothermal Technique at 90 C˚ from 350 to 480 nm at a different mole percentage of yttrium.

The direct band gap energies of the non-doped and Y-doping ZnO NRs samples were estimated using the Tauc equation $\alpha h\nu = A(h\nu - E_g)^r$, as shown in Figure 8A. The differences in $(\alpha h\nu)^2$ versus the photon energy $(h\nu)$ in the fundamental absorption region are plotted in Figure 9A. Extrapolation of the linear portion to the energy axis at $(\alpha h\nu)^2 = 0$ gives the band gap (Eg) value. The band gap energy's value is gradually decreased from 3.23 eV to 3.19 eV for mole percentage of $0 \leq Y \leq 2.2\%$ as shown in Figure 8B. The revealed lower band gap of Y doped ZnO than bulk ZnO NRs (3.23eV). The band gap energies of ZnO NRs and Y-doped ZnO NRs with different mol percentages of 0.4, 0.8, 1.2 and 2.2 were estimated to be 3.23, 3.22, 3.20, 3.19, and 3.18 eV, respectively. And some reported similar band gaps narrowing observation for Y-doped ZnO nanostructures [27].
These results are described by the incorporation of the Y^{3+} into a native ZnO NRs lattice. The doping process forms new energy levels within the normal ZnO band gap structure. As Yttrium is a tri-valence ion, doping it into ZnO lattice could release more electrons; the residual electrons in turn could re-strain the formation of defects which also supply excess electron since the ionic radius of Y^{3+} is bigger than that of Zn^{2+}. As increased in the Y dopant percentage, the electron density overlaps will increase. This will cause the split in the donor energy level and broaden into an impurity band [27].

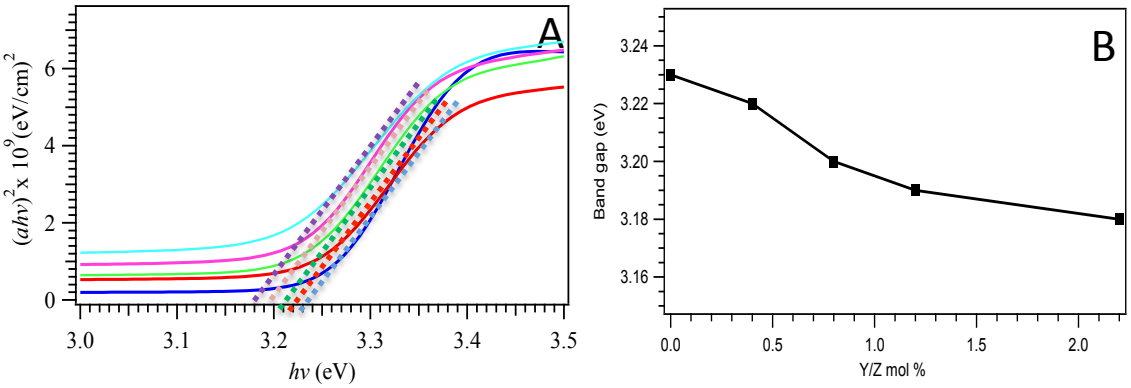

Figure 8. (A) The $(\alpha h\nu)^2$ versus $(h\nu)$ curves of ZnO and YZO Nanorods with various Y/Zn molar ratios, and (B) plot of band gap as a function of Y mol percentage.

3.4. Electrical Properties

The electrical properties were investigated by a four-point probe measurement. The electrical conductivity and resistivity of ZnO NRs and Y-doped ZnO NRs with a different mole percentage of Y as a function of various %Y contents are shown in Figure 9. The electrical conductivity and resistivity of the sample can be calculated using the following equations.

$$\rho = R \times t \quad (6)$$

$$\sigma = {}^{1}/_{\rho} \quad (7)$$

Where ρ is the electrical resistivity (Ω cm), R is the sheet resistance (Ω), t is the film thickness (cm) and σ is the conductivity (S.cm^{-1}).

Table 1. The electrical conductivity and resistivity of ZnO NRs and Y-doped ZnO NRs with different Y/Z mol%.

Y/Z mol %	Volt (V)	Ampere (A)	R (Ω)	ρ (Ω cm)	σ (S cm^{-1}).
0%	2.034	3.62 x 10^{-6}	561878.45	89.90	0.011123
0.4%	1.52	2.71 x 10^{-5}	56088.56	9.92	0.100806
0.8%	0.419	8.5 x 10^{-5}	492.94	0.936	1.06837
1.2%	0.203	7.2 x 10^{-4}	281.944	0.0761	13.14060
2.2%	2.384	3.3 x 10^{-5}	72242.42	15.89	0.06293

As shown in Figure 9A, the electrical resistivity first decreased with increasing Y contents. A minimum electrical resistivity of 0.0761 Ω cm and maximum electrical conductivity 13.14060 was obtained at a doping content of 1.2 mole% as shown in Table 1. However, as the Y/Zn molar ratio is above 1.2%, the electrical resistivity of the samples started to increase and conductivity started to decrease as a result, which suggest that when a small amount of Y is introduced, it ionizes to Y^{3+} and can easily be substituted for a Zn^{2+} site without pronounced lattice distortion. This substitution generates an extra free electron in the conduction band, thereby increasing electrical conductivity. By increasing the doping concentration further, the conductivity decreases because of grain boundary scattering of the carriers and segregation of Y at the grain boundaries. The decrease of the conductivity as the Y doping content exceed 1.2% Y/Zn molar ratio suggests that not all the Y atoms in the ZnO film are contributed to the donor dopants.

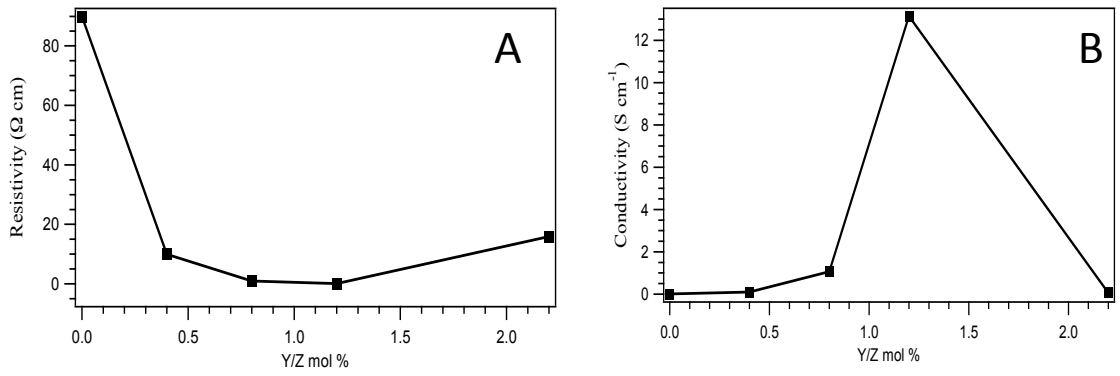

Figure 9. Variation of resistivity and conductivity of the Y-doped ZnO films as a function of Y molar percentage at 90C˚ (A) Electrical resistivity and (B) conductivity.

3.5. PEC Water Splitting Properties

The PEC water splitting performances of the ZnO NRs and YZO NRs were investigated. The PEC measurements were conducted in 1.0 M KOH electrolyte (pH=13.6). Figure 11A shows the photocurrent densities of 0.25, 0.50, 0.65, 1.20, and 0.419 mA cm^{-2}, and were obtained for pure ZnO NRs and Y-doped ZnO NRs with different mole percentages of 0, 0.4, 0.8, 1.2 and 2.2., respectively, against the Ag/AgCl. It is obvious that Y- doped ZnO NRs samples of (0.4, 0.8 and 1.2 mol %) yielded photocurrent density at least three times higher than that of pristine ZnO nanorods. The maximum photocurrent density of (1.2 mA/cm^2) (at 0.2 V vs. Ag/ AgCl) was achieved using the sample of 1.2 mol% of yttrium. The significant enhancement of photocurrent density is due to the following reasons: Firstly, incorporating yttrium ions into the ZnO NR lattice forms sub-band states within the band gap of ZnO. Secondly, oxygen defect band states are also created within the band gap; the electrons are not directly excited to the conduction band. The sub-band states may capture electrons and prevent them from the recombination with holes. Subsequently, the lifetime of the excited electrons is increased and their initial excitation into the conduction band is supported, which increases their availability for involvement in photocatalytic reactions, the precise level of the doping is a key factor.

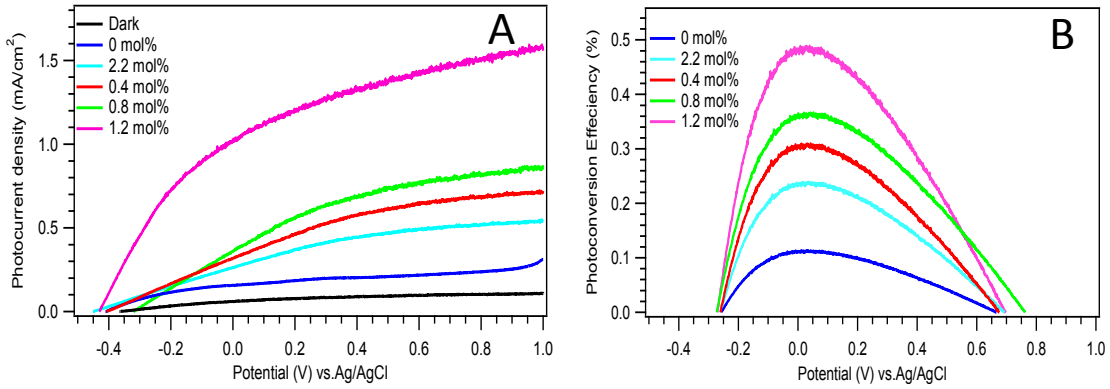

Figure 10. PEC parameters: (A) photocurrent density-voltage (J-V) characteristic and (B) photocurrent conversion efficiency % (PCE). For ZnO and YZO NRs in 1.0 M KOH electrolyte (pH 13.6) under simulated sunlight of 100 mW.cm^{-2} with an AM1.5 G filter.

However, as the Y/Zn molar ratio is above 1.2%, the photocurrent density of the samples started to decrease, this suggest that high doping concentration creates high levels of defects, which act as charge carrier recombination centers. This leads to reducing the photocatalytic activity. The photoconversion efficiency of the sample can be calculated from the ratio of electrochemical energy density to the input of photo energy density, as presented in Figure 10B. The maximum photoconversion efficiencies are 0.12 for ZnO and are 0.24, 0.33, 0.40, and 0.34% for Y-doped ZnO NRs. The higher photoconversion efficiencies suggest that the Y-doped ZnO NRs electrodes are more efficient in light absorption and converting it to the electricity than the pure ZnO NRs electrode.

4. Conclusion

This chapter demonstrated a facile preparation of the controlled incorporation of Y ions into vertically aligned crystalline YZO NR arrays by hydrothermal method at 90 °C for 130 min. The incorporation of yttrium ion into the host lattice was achieved and proved by XRD data. The surface morphology of the NRs is strongly affected by the Y/Zn molar ratio. The introduction of Y atoms into ZnO lattice will cause the change in both the optical and electrical properties of the NRs. However, Doping with Y^{3+} ion induces band gap narrowing from 3.38 eV to 3.18 eV in ZnO as they create an impurity band in the visible wavelength region and thus, exhibit properties similar to those of metal nanoparticles. PEC measurements reveal that photocurrent density reached 1.2 $mAcm^{2-}$ at 0.2 V vs. Ag/ AgCl for 1.2 mol

fraction of yttrium, which is three times higher than that of the non-doped film. This performance corresponded to a calculated photo efficiency of 0.4% at -0.38 V vs. Ag/AgCl. The efficiency, reduced significantly by increasing the doping concentration up to 1.2 mol%.

5. References

1. Willander M 2009 Zinc oxide nanorod based photonic devices: recent progress in growth, light emitting diodes and lasers. Nanotechnology, 20(33): p. **332001**.
2. Nickel H and Terukov E 2006 Zinc Oxide-A Material for Micro-and Optoelectronic Applications: Proceedings of the NATO Advanced Research Workshop on Zinc Oxide as a Material for Micro-and Optoelectronic Applications, held in St. Petersburg, Russia, Vol. 194.: Springer Science & Business Media.
3. Yang X 2009 Nitrogen-doped ZnO nanowire arrays for photoelectrochemical water splitting. Nano Letters, 9(6): p. **2331-2336**.
4. Qi J 2006 Doping and defects in the formation of single-crystal ZnO nanodisks. Applied physics letters, 89(25): p. **252115**.
5. Fan Z 2009 Toward the development of printable nanowire electronics and sensors. Advanced Materials, 21(37): p. **3730-374**3.
6. Kim D, Yun I and Kim H 2010 Fabrication of rough Al doped ZnO films deposited by low pressure chemical vapor deposition for high efficiency thin film solar cells. Current Applied Physics, 10(3): p. **S459-S462**.
7. Anota C 2013 First-principles investigation of the interaction between BN, SiC and ZnO nanotubes-$BaTiO_3$. Superlattices and Microstructures, **63**: p. 298-305.
8. Yan H 2003 Dendritic nanowire ultraviolet laser array. Journal of the American Chemical Society, 125(16): p. **4728-4729**.
9. Vayssieres L 2003 Growth of arrayed nanorods and nanowires of ZnO from aqueous solutions. Advanced Materials, 15(5): p. **464-466**.
10. Tong Y 2007 Growth and optical properties of ZnO nanostructures by vapor transport process. Materials chemistry and physics, 103(1): p. **190-19**4.
11. Tiwari J 2013 Reduced graphene oxide-based hydrogels for the efficient capture of dye pollutants from aqueous solutions. Carbon, 56: p. **173-182**.
12. Chen K 2014 Quantum-Dot-Sensitized Nitrogen-Doped ZnO for Efficient Photoelectrochemical Water Splitting. European Journal of Inorganic Chemistry, (4): p. **773-779**.
13. Liu Y 2015 Design of sandwich-structured ZnO/ZnS/Au photoanode for enhanced efficiency of photoelectrochemical water splitting. Nano Research, **8**(9): p. **2891-2900**.
14. Ilican S 2013 Effect of Na doping on the microstructures and optical properties of ZnO nanorods. Journal of Alloys and Compounds, 553: p. **225-23**2.
15. Wang F 2014 Cl-Doped ZnO Nanowires with Metallic Conductivity and Their Application for High-Performance Photoelectrochemical Electrodes. ACS Applied Materials & Interfaces,. 6(2): p. **1288-1293**.
16. Downing M, Ryan M and McLachlan M 2013 Hydrothermal growth of ZnO nanorods: The role of KCl in controlling rod morphology. Thin Solid Films, 539: p. **18-22**.
17. Han X, Han K and Tao M 2010 Low resistivity yttrium-doped zinc oxide by electrochemical deposition. Journal of the Electrochemical Society, 157(6): p. **H593-H597**.
18. Hammad M, Salem K and Harrison R 2009 Synthesis, characterization, and optical properties of Y-doped ZnO nanoparticles. Nano, 4(04): p. **225-232**.
19. Sanoop P 2012 Synthesis of yttrium doped nanocrystalline ZnO and its photocatalytic activity in methylene blue degradation. Arabian Journal of Chemistry.
20. Kim S 2013 Effects of doping with Al, Ga, and In on structural and optical properties of ZnO nanorods grown by hydrothermal method. Bulletin of the Korean Chemical Society, 3**4**(4): p. **1205-1211**.

21. Baruah S and Dutta J 2009 Hydrothermal growth of ZnO nanostructures. Science and Technology of Advanced Materials, **10**(1): p. 013001.
22. Joo J 2011 Face-selective electrostatic control of hydrothermal zinc oxide nanowire synthesis. Nature materials, 10(8): p. **596-601.**
23. Zheng J 2012 Enhanced UV emission of Y-doped ZnO nanoparticles. Applied Surface Science,. 258 (18): p. **6735-6738**.
24. Shannont H 1976 Revised effective, ionic radii and systematic studies of interatomic distances in halides and chalcogenides. Acta crystallographica section A: crystal physics, diffraction, theoretical and general crystallography, 32 (5): p. **751-767**.
25. Ryu Y, Lee T and White H 2003 Properties of arsenic-doped p-type ZnO grown by hybrid beam deposition. Applied physics letters, 83(1): p. **87-89**.
26. Yogamalar R 2012 Dopant induced bandgap narrowing in Y-doped zinc oxide nanostructures. Journal of nanoscience and nanotechnology, 12(1): p. **75-83**.
27. Yu Q 2007 Structural electrical and optical properties of yttrium-doped ZnO thin films prepared by sol–gel method. Journal of Physics D: Applied Physics, 40(18): p. **5592**.